Supplement of Atmos. Chem. Phys., 22, 2669–2687, 2022
https://doi.org/10.5194/acp-22-2669-2022-supplement

Atmospheric Chemistry and Physics
Open Access
EGU

Supplement of

Comparison of six approaches to predicting droplet activation of surface active aerosol – Part 1: moderately surface active organics

Sampo Vepsäläinen et al.

Correspondence to: Nønne L. Prisle (nonne.prisle@oulu.fi)

Introduction

This document provides additional results, more detail on the calculations and thermodynamical data used in the calculations with some of the models. A sensitivity analysis with regards to various parameters and models at $w_{\mathrm{p,org}} = 0.95$ is also provided.

S1 Additional results

The following sections contains the variations of supersaturation, surface tensions and the organic bulk–surface partitioning factors along Köhler curves predicted with the different models for particles of succinic and glutaric acids mixed with ammonium sulfate. Table S1 contains properties of the organic acids as pure compounds including molar mass, density in solid phase, density and surface tension in a hypothetical supercooled liquid state. The results presented here are for with dry particle size of $D_{\mathrm{p}} = 50$ nm at organic mass fractions ($w_{\mathrm{p,org}}$) of 0.2, 0.5, 0.8 and 0.95 all at 298.15 K for all the different model calculations.

S1.1 Succinic acid

Table S2 shows the droplet properties at the critical point (diameter, surface tension and supersaturation) predicted with different models in the case of succinic acid–ammonium sulfate particles.

Figure S1 shows the Köhler curves predicted with the different models for particles containing succinic acid. These results show similar trends to those of malonic acid. In Figs. S1(c) and S1(d), the curve predicted with the partial organic film model shows a larger discrepancy after the surface coverage of the organic film becomes partial compared to the curves predicted with the monolayer, Gibbs and bulk solution models than it did with the curve predicted for particles containing malonic acid. The discrepancy is still not large.

Figure S2 shows the surface tensions predicted with the different models along the Köhler curves for simulations with succinic acid. These results are similar in appearance and behavior to those of malonic acid.

Figure S3 shows the organic surface partitioning factors predicted with the different models for the simulations with succinic acid. These results show similar trends to those of malonic acid. Aside from the differences in the shape of the curves and intersection point between the curves predicted with the monolayer and Gibbs models, the main difference is that at low organic mass fraction in Fig. S3(a), the monolayer model predicts considerably stronger partitioning at small droplet sizes than in the case with malonic acid. In addition, the partitioning predicted with the Gibbs model becomes stronger compared to the monolayer model even in Fig. S3(a), something that does not occur with malonic acid.

S1.2 Glutaric acid

Table S3 shows the droplet properties at the critical point (diameter, surface tension and supersaturation) predicted with different models in the case of glutaric acid–ammonium sulfate particles.

Figure S4 shows the Köhler curves predicted with the different models for particles containing glutaric acid. The overall behavior of the curves show similar trends to those observed in the simulations with the other two compounds. In Figs. S4(c) and S4(d), the curve predicted with the partial organic film model after the film breaks and the group of monolayer, Gibbs and bulk model curves do not match as well as in the case of the malonic acid simulations. This behavior is similar to Fig. S1

Table S1. The molar masses (M), liquid and solid densities (ρ_{l} and ρ_{s}) and surface tensions (σ) of succinic and glutaric acids at 298.15 K, unless stated otherwise.

Compound	M ($\mathrm{g\,mol^{-1}}$)	ρ_{l} ($\mathrm{kg\,m^{-3}}$)	ρ_{s} ($\mathrm{kg\,m^{-3}}$)	σ ($\mathrm{mN\,m^{-1}}$)
Succinic acid	118.089	1470.73[a]	1572.0[b]	47.67[c]
Glutaric acid	132.116	1274.48[d]	1429.0[b] (288.15 K)	50.76[e]

[a] Hyvärinen et al. (2006) [b] CRC Handbook (1988) [c] Vanhanen et al. (2008) [d] Extended from Cai et al. (2015), [e] Extended from binary fit based on measurements by Bzdek et al. (2016)

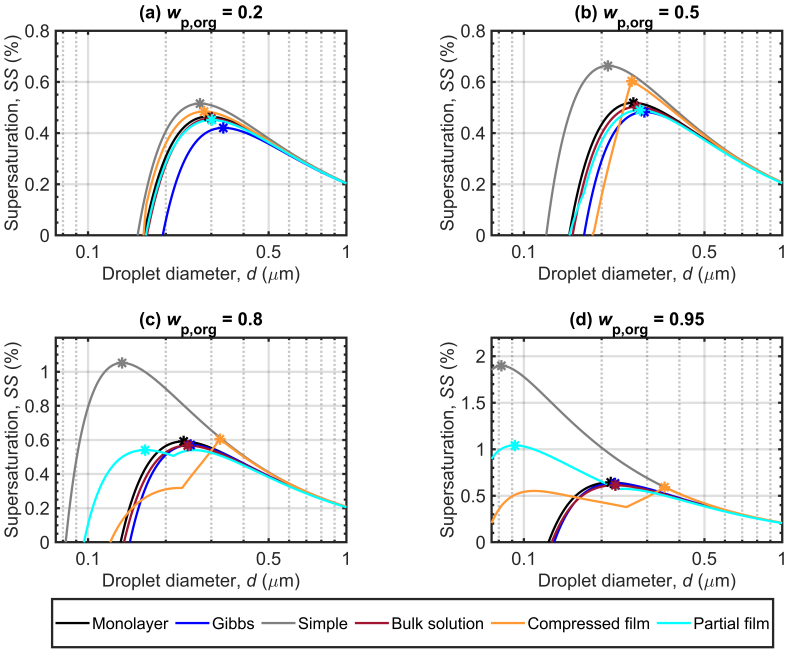

Figure S1. Köhler curves calculated with the different models for dry succinic acid–ammonium sulfate particles with $D_\mathrm{p} = 50$ nm. Each panel shows curves for particles with a different succinic acid mass fraction ($w_\mathrm{p,org}$). The critical points are marked on each curve. Note that the vertical axis scaling changes between the panels.

Table S2. The critical droplet diameters (d_c), supersaturations ($\mathrm{SS_c}$) and surface tensions (σ_c) predicted with the different models in simulations for mixed succinic acid–ammonium sulfate particles of D_p = 50 nm at 298.15 K.

Parameter	d_c (nm)	$\mathrm{SS_c}$ (%)	σ_c ($\mathrm{mN\,m^{-1}}$)	d_c (nm)	$\mathrm{SS_c}$ (%)	σ_c ($\mathrm{mN\,m^{-1}}$)	d_c (nm)	$\mathrm{SS_c}$ (%)	σ_c ($\mathrm{mN\,m^{-1}}$)
$w_\mathrm{p,org}$		Monolayer			Gibbs			Simple	
0.2	292.82	0.46	71.16	333.98	0.42	71.4	271.19	0.52	71.97
0.5	265.31	0.52	70.32	292.82	0.48	70.66	211.54	0.66	71.97
0.8	234.32	0.59	69.47	249.34	0.57	69.72	135.46	1.05	71.97
0.95	217.02	0.64	69.02	225.09	0.63	69.15	81.82	1.9	71.97
$w_\mathrm{p,org}$		Bulk solution			Compressed film			Partial organic film	
0.2	300.4	0.46	71.07	281.28	0.48	71.97	301.5	0.45	68.71
0.5	274.18	0.5	70.26	261.46	0.6	71.97	281.28	0.49	62.77
0.8	243.04	0.57	69.46	324.36	0.6	71.97	166.22	0.54	47.67
0.95	225.92	0.61	69.04	350.22	0.59	71.97	92.31	1.04	47.67

with the succinic acid simulations. In addition, it appears that with the glutaric acid simulation, the curve predicted with the compressed film model intercepts the partial organic film curve very near the point of the surface film breaking in the case of Figs. S4(b), S4(c) and S4(d). As this does not happen with the other test systems, it may be an insignificant detail.

Figure S5 shows the surface tensions predicted with the different models along the Köhler curves for particles containing glutaric acid. The results again show similar trends to the other compounds. Figs. S5(b), S5(c) and S5(d) show that the predicted surface tension curves of the compressed film model and partial organic film intercept near the point where the organic film

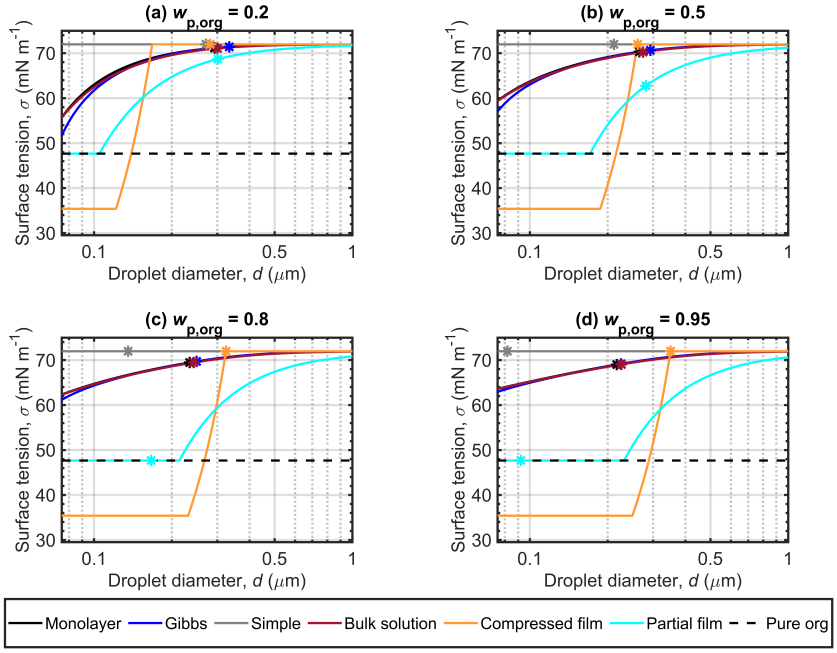

Figure S2. Surface tensions of droplets along the Köhler curves, calculated with the different models for dry particles of $D_\mathrm{p} = 50$ nm at different succinic acid mass fractions ($w_\mathrm{p,org}$) in the different panels. The critical points evaluated for the Köhler curves in Fig. S1 are also marked, and the surface tension of pure succinic acid estimated according to Vanhanen et al. (2008) is indicated as a physical lower limit for the droplet surface tension.

Table S3. The critical droplet diameters (d_c), supersaturations ($\mathrm{SS_c}$) and surface tensions (σ_c) predicted with the different models in simulations for mixed glutaric acid–ammonium sulfate particles of D_p = 50 nm at 298.15 K.

Parameter	d_c (nm)	$\mathrm{SS_c}$ (%)	σ_c (mN m^{-1})	d_c (nm)	$\mathrm{SS_c}$ (%)	σ_c (mN m^{-1})	d_c (nm)	$\mathrm{SS_c}$ (%)	σ_c (mN m^{-1})
$w_\mathrm{p,org}$		Monolayer			Gibbs			Simple	
0.2	288.57	0.47	71.37	329.13	0.43	71.57	268.24	0.52	71.97
0.5	253.93	0.54	70.49	278.22	0.51	70.89	206.2	0.68	71.97
0.8	219.41	0.63	69.13	226.74	0.63	69.54	131.08	1.09	71.97
0.95	199.53	0.7	68.1	200.26	0.72	68.34	80.05	1.96	71.97
$w_\mathrm{p,org}$		Bulk solution			Compressed film			Partial organic film	
0.2	292.82	0.47	71.31	278.22	0.49	71.97	298.22	0.46	68.68
0.5	262.42	0.53	70.44	216.23	0.64	71.97	274.18	0.5	62.71
0.8	230.92	0.61	69.17	264.35	0.72	71.83	154.5	0.62	50.76
0.95	213.09	0.66	68.27	284.38	0.73	71.97	87.7	1.18	50.76

breaks in the latter model. This does not happen with the other two compounds. Table S3 shows that in Fig. S5(c), σ_c of the predicted surface tension with compressed film model is slightly below that of pure water. There is no clear indication why this happens and could be due to some numerical glitch.

Figure S6 shows the organic surface partitioning factor for the different models for the simulations with glutaric acid. Notably, the partitioning predicted with the Gibbs model is noticeably stronger than for the other two acids. This is also true

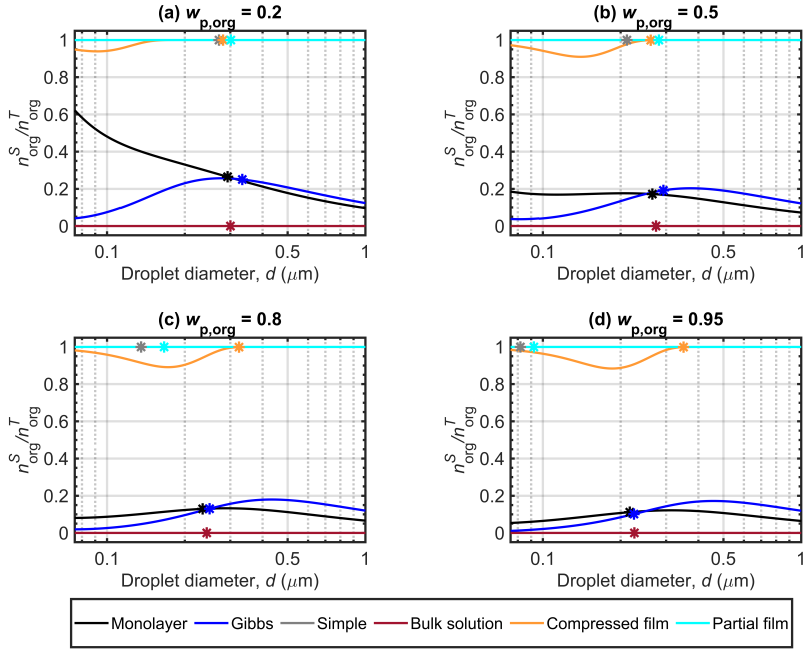

Figure S3. Succinic acid surface partitioning factors ($n^{\mathrm{S}}_{\mathrm{org}}/n^{\mathrm{T}}_{\mathrm{org}}$) predicted with the different models along the Köhler curves for dry particles with $D_{\mathrm{p}} = 50$ nm at different organic mass fractions ($w_{\mathrm{p,org}}$) in the different panels. The critical points are also marked.

for the monolayer model predictions though to a smaller degree. In addition, the compressed film model has a partitioning factor practically equal to unity the whole time, the minimum value out of all organic mass fractions is 0. 0.9984 for $w_{\mathrm{p,org}}$ = 0.95 simulation.

S1.3 Surface thickness

Figure S7 shows the monolayer thickness modeled with the monolayer model of Malila and Prisle (2018) at different organic mass fractions ($w_{\mathrm{p,org}}$) for malonic, succinic and glutaric acids. At the point of activation, the predicted surface thickness is 0.39 - 0.4 nm for all acids.

S2 Calculation details

The following sections contain details relating to the calculation of amounts of salt, organic and water as well as water activity in the droplets.

S2.1 Amount of organic and salt molecules

Amount of organic and salt molecules are calculated with the assumption of spherical particles ($V_{\mathrm{p}} = \frac{\pi}{6} D_{\mathrm{p}}^3$) and additive solid phase volumes. Starting from the definition of the organic mass fraction ($w_{\mathrm{p,org}}$), the relation between the initial salt and organic mass in the dry particle can be solved as

$$m^i_{\mathrm{salt}} = \frac{(1 - w_{\mathrm{p,org}}) m^i_{\mathrm{org}}}{w_{\mathrm{p,org}}}. \tag{S1}$$

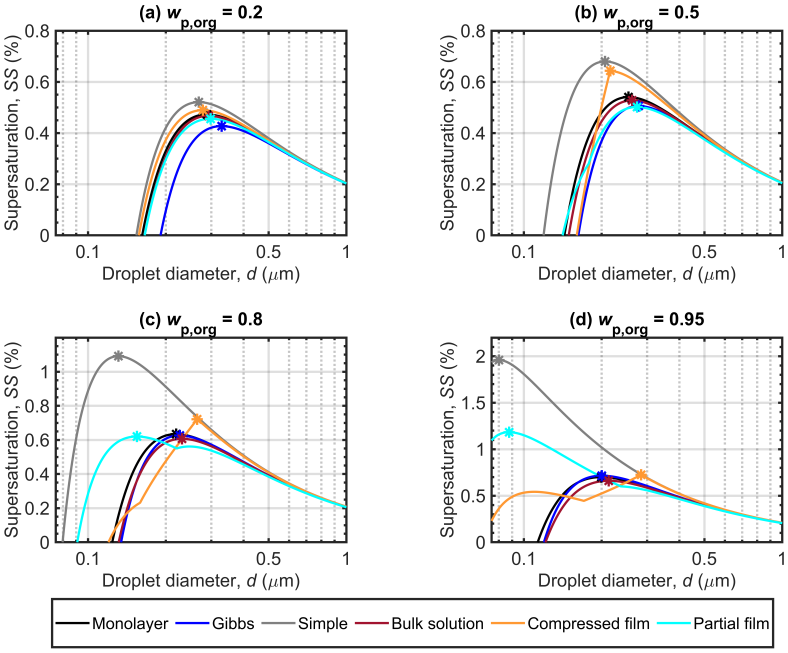

Figure S4. Köhler curves calculated with the different models for dry glutaric acid–ammonium sulfate particles with $D_\mathrm{p} = 50$ nm. Each panel shows curves for particles with a different glutaric acid mass fraction ($w_{\mathrm{p,org}}$). The critical points are marked on each curve. Note that the vertical axis scaling changes between the panels.

The initial mass of organic in the particle can be derived starting with the basic equation $m^i_\mathrm{org} = V_\mathrm{org}\rho^\mathrm{s}_\mathrm{org}$. Solving for V_org and substituting it in terms of volume fraction and the particle volume, and then writing out the volume fraction in terms of initial masses and solid phase densities ($\rho^\mathrm{s}_\mathrm{org}$ and $\rho^\mathrm{s}_\mathrm{salt}$) and making use of Eq. (S1) finally leads the equation for the initial the organic mass

$$m^i_\mathrm{org} = \frac{V_\mathrm{p}}{\frac{1}{\rho^\mathrm{s}_\mathrm{org}} + \frac{(1-w_{\mathrm{p,org}})}{w_{\mathrm{p,org}}\rho^\mathrm{s}_\mathrm{salt}}}. \tag{S2}$$

The initial amounts of molecules can then be calculated by dividing Eqs. (S1) and (S2) with the corresponding molecular mass $m_j = M_j/N_\mathrm{A}$.

The compressed film model (Ruehl et al., 2016) employs different equations but with the same assumptions (see Ruehl et al. (2016) supplement), using a salt seed particle covered by an organic layer.

S2.2 Amount of water molecules

Calculations with the assumption of additive volumes of the dry particle and of the water condensed on it follow equation (or a similar equivalent one)

$$n^\mathrm{T}_\mathrm{w} = \frac{\rho_\mathrm{w}}{M_\mathrm{w}}\frac{\pi}{6}\left(d^3 - D^3_\mathrm{p}\right)N_\mathrm{A}, \tag{S3}$$

where ρ_w is the density of water, M_w the molar mass of water, d the droplet diameter, D_p the dry particle diameter and N_A Avogadro's number.

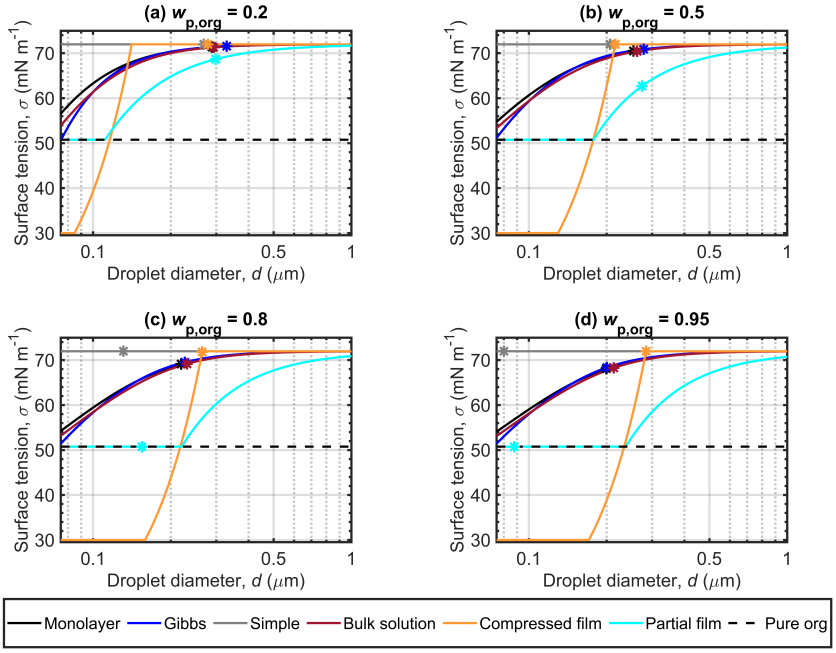

Figure S5. Surface tensions of droplets along the Köhler curves, calculated with the different models for dry particles of $D_\mathrm{p} = 50$ nm at different glutaric acid mass fractions ($w_{\mathrm{p,org}}$) in the different panels. The critical points evaluated for the Köhler curves in Fig. S4 are also marked, and the surface tension of pure glutaric acid estimated though extending the binary fit of Bzdek et al. (2016) is indicated as a physical lower limit for the droplet surface tension.

For the iterative method based on mass conservation using the solution density, the following equation

$$\left| \frac{\pi}{6} \pi d^3 \rho(x,T) - n_\mathrm{w}^\mathrm{T} m_\mathrm{w} - n_\mathrm{org}^\mathrm{T} m_\mathrm{org} - n_\mathrm{salt}^\mathrm{T} m_\mathrm{salt} \right| = 0 \tag{S4}$$

is solved for n_w^T using Matlab function *fsolve* where ρ is the composition dependant liquid solution density, x is a mole fraction matrix containing water, organic and salt and m_j is the molecular mass of compound j (water, organic, salt). Whatever moles or the number of molecules are used for calculations varies between the models.

S2.3 Water activity

The water activity in ternary droplet solutions is calculated as the corrected mole fraction according to equation

$$a_\mathrm{w} = \frac{n_\mathrm{w}}{n_\mathrm{w} + i_\mathrm{salt} n_\mathrm{salt} + i_\mathrm{org} n_\mathrm{org}}, \tag{S5}$$

where $n_\mathrm{w}, n_\mathrm{salt}$ and n_org are the number of molecules of water, salt and organic, i_salt is the van't Hoff factor for salt, and i_org for the organic. Frosch et al. (2011) found that water activities of organic-inorganic aqueous mixtures similar to the droplets of the present work were mainly influenced by the presence of inorganic salts due to the higher degree of dissociation of the salt. Therefore, we here assume van't Hoff factors of unity for each of the organics and for ammonium sulfate, the van't Hoff factor is calculated as

$$i_\mathrm{salt} = \max(-0.007931\,(\ln b_\mathrm{salt})^2 - 0.1844 \ln b_\mathrm{salt} + 1.9242, 1.9242) \tag{S6}$$

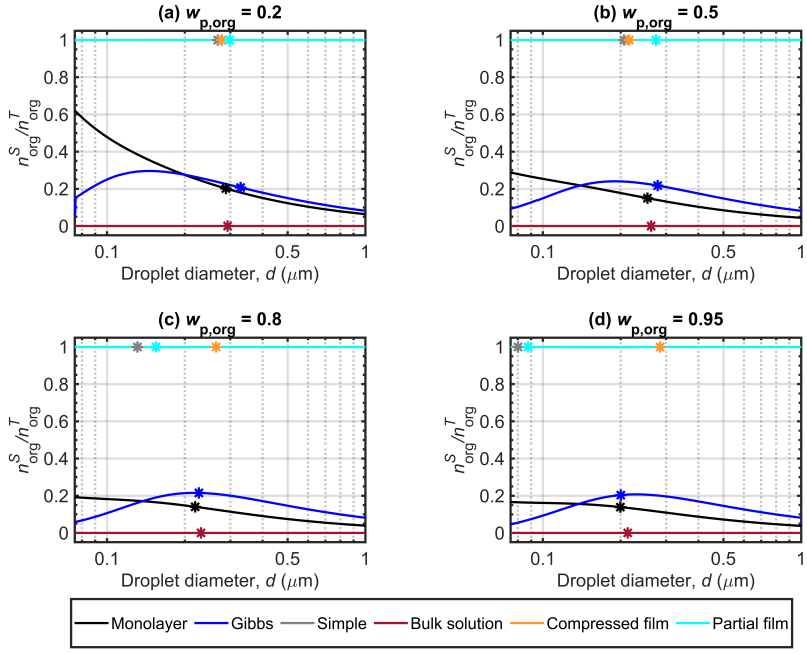

Figure S6. Glutaric acid surface partitioning factors ($n^{\mathrm{S}}_{\mathrm{org}}/n^{\mathrm{T}}_{\mathrm{org}}$) predicted with the different models along the Köhler curves for dry particles with $D_{\mathrm{p}} = 50$ nm at different organic mass fractions ($w_{\mathrm{p,org}}$) in the different panels. The critical points are also marked.

where b_{salt} is the f the molality of ammonium sulfate. The equation has been restricted in case of molality values outside of the region it was intended for (Young and Warren, 1992).

To calculate the water activity for the binary systems of salt (ammonium sulfate) and water in the simple model, a fit (Prisle, 2006) is used. It gives the activity as

$$a_{\mathrm{w}} = 1 - 0.039767 b_{\mathrm{salt}} + 0.0079808 b^2_{\mathrm{salt}} - 0.0022641 b^3_{\mathrm{salt}}. \tag{S7}$$

The AIOMFAC based (AIOMFAC-web, 2020) fit used for the partial organic film model (Ovadnevaite et al., 2017) is

$$a_{\mathrm{w}} = 0.0011 \cdot \exp(-7.0930 \cdot 10^2 \cdot x_{\mathrm{salt}}) + 0.9989 \cdot \exp(-1.8762 \cdot x_{\mathrm{salt}}) \tag{S8}$$

where x_{salt} is the mole fraction of ammonium sulfate. The fit was done at 298.15K.

S2.4 Compressed film model parameters

Table S4 contains the model parameters used for the calculations with the compressed film model of Ruehl et al. (2016). This study does not contain new fittings of the parameters. However, it should be noted that when fitting the parameters, the properties of growing droplets are quite different at lower sub-saturation RH values and near the critical point. For good parameters, one should have data at sufficiently high supersaturation making such data somewhat difficult to acquire as all D_{seed}, D_{p} and d are needed in addition to the RH. The fitting happens to the droplet sizes before activation (the rising part of the Köhler curve) at one organic fraction like Ruehl et al. (2016), or across several organic fractions at one RH value like Forestieri et al. (2018). Assuming that the parameters are physical constants, they can be applied to a range of conditions.

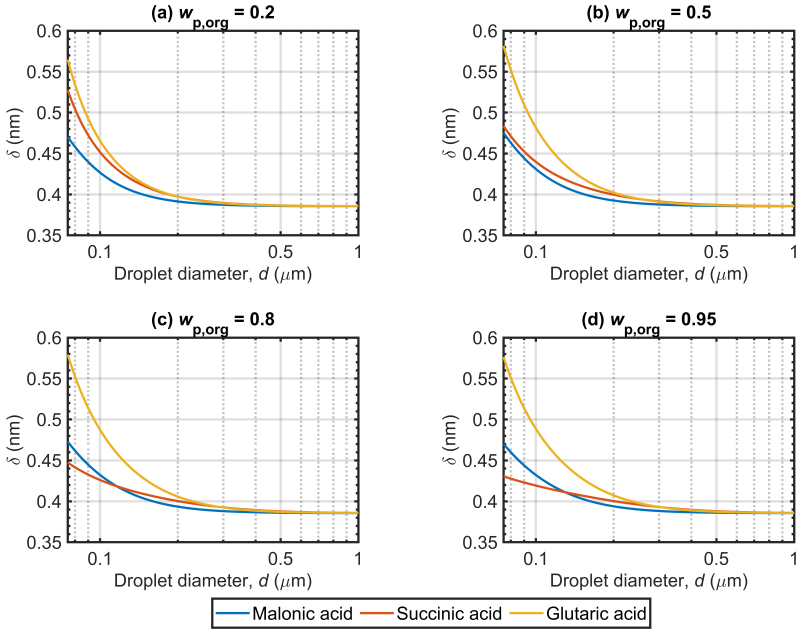

Figure S7. The droplet surface layer thickness along the Köhler curve predicted with the monolayer model of Malila and Prisle (2018) for $D_\mathrm{p} = 50$ nm at different organic mass fractions ($w_\mathrm{p,org}$) in the different panels for particles of ammonium sulfate mixed with malonic, succinic and glutaric acids.

Table S4. Compressed film model parameters used for in the calculations for the different organic compounds. All values were taken from Ruehl et al. (2016).

Compound	A_0 (Å^2)	m_σ (mJ m^{-2} Å^{-2})	$\log_{10} C_0$	σ_min (mN m^{-1})
Malonic	71.2	1.13	-6.1	32.4
Succinic	76.9	1.04	-6.2	35.4
Glutaric	62	1.06	-7	30

S3 Sensitivity analysis

The sensitivity analysis was done via single parameter perturbations (OAT analysis) with the same conditions as the main simulations (D_p = 50 nm and $T = 298.15$ K) for organic mass fraction of $w_\mathrm{p,org} = 0.95$ in the initial particles. The analysis done with fitting parameters is provided for particles containing malonic, succinic and glutaric acids while analysis for non-fitting parameters (used as compound specific constants) is only provided for particles containing malonic acid. This is because variations in the fitting parameters could lead to significantly different results depending on the original fitting conditions and data, as well as the goodness of the fit, and could therefore be very compound specific. The compound specific constants behave the same for all compounds and variations to them are therefore expected to produce similar results for each of the investigated acids. While the compressed film model parameters are assumed to be compound specific physical constants during the simulations, they were originally acquired through fitting, and are therefore tested here for particles containing each of the investigated acids.

Table S5. Change in the compressed film model parameters (Table S4) needed to change the critical point to the second visible maxima. The changes were done as multipliers to the indicated parameters as for example $A_0 \cdot X$ where X is the multiplier taken as $(100\% \pm \Delta\%)/100$. The tabulated values correspond to $\Delta\%$.

Compound	A_0 (Å^2)	m_σ (mJ m^{-2} Å^{-2})	$\log_{10} C_0$	$\sigma_{\min}$ (mN m^{-1})
Malonic	-52.0%	-34.5%	+16.5%[a]	+9.1%
Succinic	-4.3%	-6.0%	+3.1%[a]	+4.2%
Glutaric	-44.7%	-36.6%	-	+21.9%

[a] The $\log_{10} C_0$ itself is negative and this was calculated as $\log_{10} C_0 \cdot X$ where X is a fraction (100% + 9.1%)/100, this is technically a smaller number

S3.1 Compressed film model specific variations

In the predicted Köhler curves for particles containing each of the investigated organic acids (Figs. 2, S1 and S4), there is a prominent second local maximum at $w_{\mathrm{p,org}} = 0.95$ (panel (d) of the Figs. 2, S1 and S4). The sensitivity analysis consists of varying the compressed film model specific parameters A_0, $\log_{10} C_0$, m_σ and $\sigma_{\min}$ to investigate whether the critical point shifts from the first to the second local maximum, which resides in a droplet region where the model specific minimum droplet surface tension is realized. Outside of this sensitivity analysis, results of each simulation presented in this work, as well as by other studies (e.g. Ruehl et al., 2016; Forestieri et al., 2018), predict that all surfactant has partitioned to the droplet surface at the point of activation, and that the droplet surface tension has reached that of pure water (or a value very close to it). If the critical point is predicted to occur at droplet conditions significantly different from these, it indicates lack of robustness in the fitting of the model parameters. Figs. S8, S9 and S10 show the results of the analysis for the Köhler curves of particles containing malonic, succinic and glutaric acid respectively. The Figs. contain 1%, 5% and 10% changes in parameters A_0, $\log_{10} C_0$, m_σ and $\sigma_{\min}$ in shaded red areas around the baseline in black. These values were chosen based on the limits given in Ruehl et al. (2016) that vary between 1.6 - 8.5% depending on the compound and the parameter. The limits where the critical point moves to the second maximum is marked in blue line and a corresponding change in the other direction is also shown. The changes to the parameters in percentage are listed in Table S5. The changes were done as multipliers to the indicated parameters as for example $A_0 \cdot X$ where X is the multiplier taken as $(100\% \pm \Delta\%)/100$. The values listed in Table S5 correspond to the $\Delta\%$.

There is a large difference in sensitivity between the compounds (Table S5). The model is very robust with malonic and glutaric acid simulations, changing the critical point to the second local maximum requiring significant changes in the parameters. Succinic acid simulation changes the location of the critical point with much smaller changes the other two compounds. This was to be expected as the second local maximum is more prominent with succinic acid (Fig. S1).

The effect of the different parameters themselves on the Köhler curves can be observed in Figs. S8, S9 and S10 for particles containing malonic, succinic and glutaric acids respectively. The molecular area A_0 always influences the critical point, as well as the point where the surface tension starts to increase. With malonic (Fig. S8) and succinic (Fig. S9) acid simulations, it affects both of the local maxima while with glutaric acid only the more prominent maximum excluding the large change needed to shift the critical point to the first maximum where the whole shape of the curve changes. Parameters $\log_{10} C_0$ and m_σ affect the first maximum but does not seem to have a significant effect on the actual critical point before the the change between the two maxima. Glutaric acid simulation is an exception again, m_σ only has a small effect on the transaction region where the surface tension changes. With $\log_{10} C_0$, the variation had no visible effect on the Köhler curve until very large variations. No change in the critical point between the two local maxima was observed. Of course, $\sigma_{\min}$ itself has a clear effect but only during small droplet sizes, never affecting the critical point before it moves to the first maximum.

Simulations with glutaric acid (Fig. S10) could exhibit their unique behavior due to glutaric acid being the most surface active of the organic compounds used. The surface partitioning factor of glutaric acid is effectively equal to unity for all the 1-10% changes. Glutaric acid is also the most soluble in water out of the compounds investigated here.

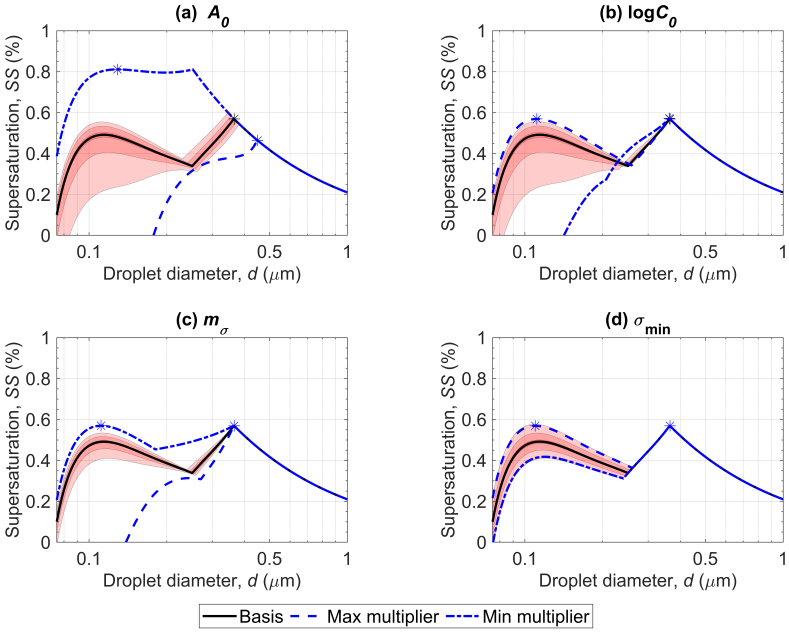

Figure S8. The sensitivity of the malonic acid supersaturation with respect to changes in each of the compressed film model parameters. The red areas match $\pm$ 1%, 5% and 10% changes while the blue lines correspond to the change in the critical point listed in Table S5.

S3.2 Partial organic film model specific variations

In this section, the surface tension of pure (supercooled) malonic acid (σ_{org}), the surface tension of pure ammonium sulfate (σ_{salt}) and the surface film thickness (δ) were varied by $\pm$ 1 %, 5 %, 10 %, 25 % and 50 %. The changes were done similarly to the previous analysis as multipliers to the indicated parameters as for example $\sigma_{\mathrm{org}} \cdot X$ where X is the multiplier taken as $(100\% \pm \Delta\%)/100$. The maximum level of variation ($\pm$50 %) was roughly chosen based on the results of the previous sensitivity analysis where the largest required absolute change to shift the critical point to the second local maxima was 52 %. The sensitivity of the Köhler curve predicted with the partial organic film model can be seen in Fig. S11, and the corresponding surface tension in Fig. S12. Variations in the liquid phase density of the organic is also included into the same Figs. as panel (a), but the related discussion comes later in section S3.4.

Variations in the surface tension of the pure organic compound, presented in the (b) panels of Figs. S11 and S12, can shift both the predicted Köhler and surface tension curves significantly. Naturally the effect is largest before the breaking of the surface film, where the surface tension of the pure organic compound is used. This can potentially modify the critical point significantly, even changing it's the location to the second local maximum if the decrease in surface tension is large enough.

Varying the surface tension of the pure salt, presented in the (c) panels of Figs. S11 and S12, does not show any significant effects under the conditions of these simulations.

Varying the surface thickness, shown in the (d) panels of Figs.S11 and S12, can shift the point of the surface film breaking, and affect the predicted Köhler curve and the surface tension in that region, but has no effect on the critical point.

S3.3 Varying ternary surface tension fitting parameters

The fitting parameters A, B, C and D in the surface tension parametrization presented in Eq. S9 and Table S6 and used by the Gibbs, monolayer and bulk solution models were varied by $\pm$ 1 %, 5 %, 10 %, 25 % and 50 %. Similarly to before, the changes

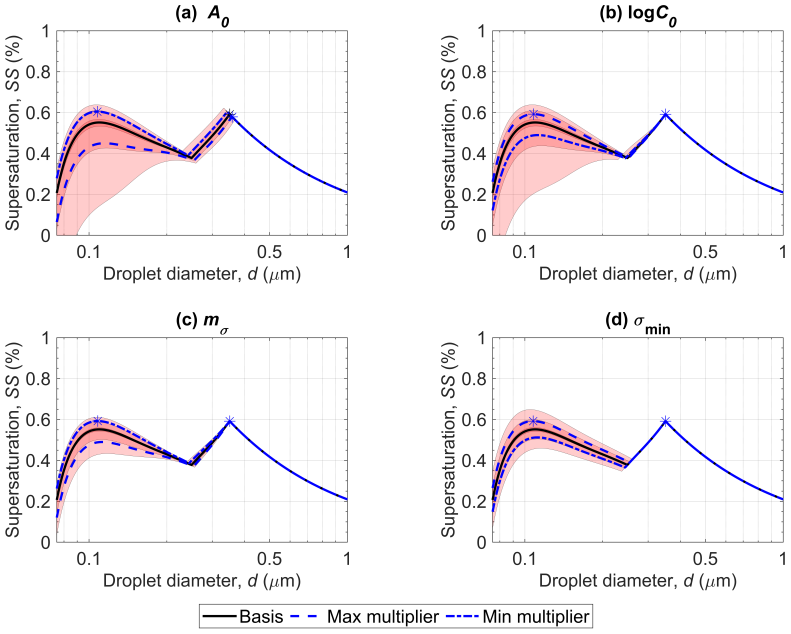

Figure S9. The sensitivity of the succinic acid supersaturation with respect to changes in each of the compressed film model parameters. The red areas match ± 1%, 5% and 10% changes while the blue lines correspond to the change in the critical point listed in Table S5.

were done as multipliers to the indicated parameters as for example $A \cdot X$ where X is the multiplier taken as $(100\% \pm \Delta\%)/100$. This sensitivity analysis was done for particles containing each of the investigated three acids at a time. As all the three models and compounds behaved similarly in regards to all variations, a representative figure of the most sensitive case was chosen and is displayed in Fig. S13.

For particles containing malonic acid, the most significant changes appear with the variations in the parameters A and B. A minor shift in the Köhler curve is visible for the bulk solution model with parameter A but disappears as the droplet size increases. The other models do not show significant differences in the Köhler curves. The surface tension shows more variation for all three models at small droplet sizes but, the differences disappear together with increasing droplet diameter. The variations in the parameters C and D do not appear to cause any visible changes in the predicted Köhler or surface tension curves.

The results for particles containing succinic acid are similar in behaviour to the case with malonic acid. The models behave similarly, with the minor exception that now variations in the parameter C cause a minuscule shift in the surface tension curve at small droplet sizes in the predictions of all three models. This difference is extremely small and disappears as the droplets increase.

The predictions with particles containing glutaric acid show the most sensitivity. There is a visible but still minor shift in the Köhler curve predictions of the bulk solution model by varying parameters A and B as can be seen in Fig. S13. A minor shift can also be seen for the Köhler curve predicted with the Gibbs model in the case parameter B variations, but not for the predictions of the monolayer model. In addition, the predicted surface tension curves are the most affected by variations in the parameters A and B, even going as far as to shift the surface tension at the smallest droplets to that of the pure organic for the predictions of all three models.

In conclusion, none of the predictions of the different models are overly sensitive to changes in the parameters of the ternary surface tension parametrization. The predictions of the bulk solution model are slightly more sensitive than the other two

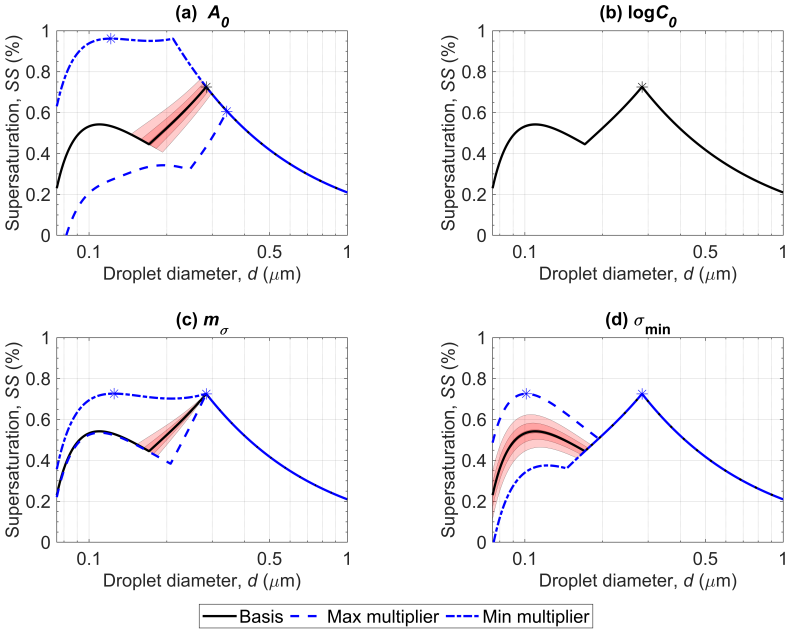

Figure S10. The sensitivity of the glutaric acid supersaturation with respect to changes in each of the compressed film model parameters. The red areas match ± 1%, 5% and 10% changes while the blue lines correspond to the change in the critical point listed in Table S5.

models. Out of the three compounds, glutaric acid predictions show the most sensitivity. Therefore the predictions of the bulk solution model with particles containing glutaric acid were chosen as to be displayed in the representative Fig. S13.

S3.4 Varying properties of the organic and salt

In this section, we varied the molar mass of the organic (M_{org}), the solid and liquid phase densities of the organic ($\rho_{\mathrm{org}}^{\mathrm{s/l}}$) and salt ($\rho_{\mathrm{salt}}^{\mathrm{s/l}}$) by ± 1 %, 5 %, 10 %, 25 % and 50 %. The changes were done as multipliers to the indicated parameters as for example $M_{\mathrm{org}} \cdot X$ where X is the multiplier taken as $(100\% \pm \Delta\%)/100$. These simulations were done with particles containing malonic acid, and predictions of all six models were tested.

Varying the molar mass of the organic, or the solid phase density of the organic or salt directly affect the composition of the dry particle, as all these quantities are used in calculating the initial number of molecules in the dry particles (Eqs. (S1) and (S2)). However, since the initial dry particles studied in this sensitivity analysis are composed mostly of organic ($w_{\mathrm{p,org}} = 0.95$), the variations in the density of the salt are expected to only produce minor differences. Generally the properties of the salt are more well known than those of the organic and therefore we give priority to the sensitivity with respect to variations in the organic properties.

For the predictions of the Gibbs, monolayer and bulk solution models, variations in the molar mass of the organic shift the Köhler curve and the critical point. The Gibbs model predictions were chosen as a representative case and Fig. S14(a) shows the Gibbs model predictions of the Köhler curve and Fig. S14(c) the surface tension along it with variations in the molar mass of the organic. From Fig. S14(a), we see the the differences are larger at smaller droplet sizes and decrease as the droplets grow. The surface tension curve in Fig. S14(c) is also affected in a similar manner and as the surface tension approaches that of water, the differences decrease. For the predictions of the compressed film model shown in Fig.S15(a), the smallest droplets are not affected but the curve in the region before the critical point as well as the critical point itself are shifted in a near linear manner. It is also possible for the critical point shift to the another local maximum if the molar mass is lowered enough as can

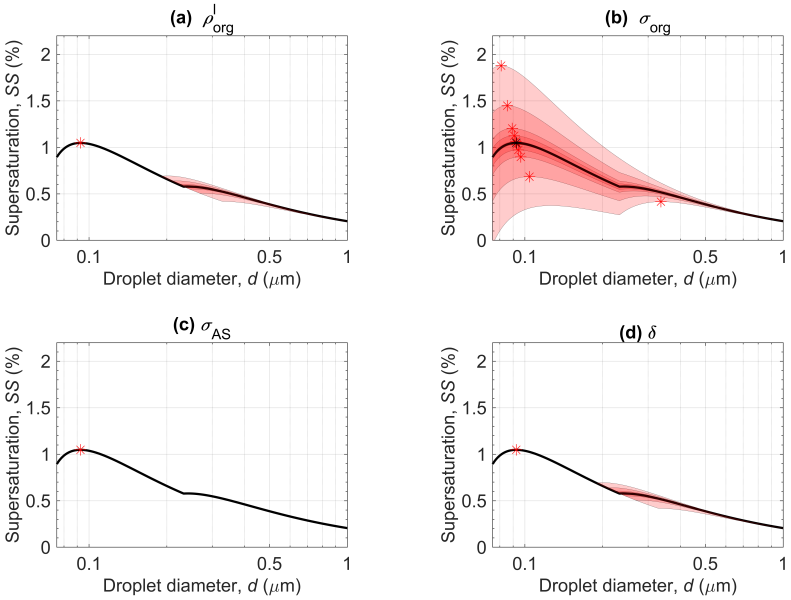

Figure S11. The sensitivity of the Köhler curve predicted with the partial organic film model with variations in the liquid density of the organic (a), the surface tension of pure organic compound (b), the surface tension of pure salt (c) and the thickness of the surface film (d) for particles containing malonic acid at $D_{\mathrm{p}} = 50$ nm and $w_{\mathrm{p,org}} = 0.95$. The red areas match $\pm$ 1 %, 5 %, 10 %, 25 % and 50 % variations in the parameters.

be seen in the Fig. S15(a). For the surface tension predictions in Fig. S15(c), only the rising part of the curve is affected by a shift in the droplet sizes at the start and ending points of the rising part of the curve. The predictions of the partial organic film and the simple model are not affected by variations in the molar mass of the organic.

Variations in the solid phase density of the organic affects the predicted Köhler curves of all models. For the Gibbs, monolayer and bulk models, the whole Köhler curve and the critical point is shifted, as is the corresponding surface tension. The Gibbs model predictions were chosen as a representative case and Fig. S14(b) and S14(d) show the predicted Köhler curve and the corresponding surface tension along it. Figs. S14(b) and S14(d) show larger differences at smaller droplet sizes that decrease with the increasing droplet size similar to the case with variations in the molar mass of the organic. For the compressed film model the whole Köhler curve up to the activation point is shifted, as is the activation point itself (Fig. S15(b)). For the surface tension predictions in Fig. S15(d) , only the rising part of the curve is affected, similarly to the case with the variations in the molar mass of the organic. For the partial organic film model shown in Figs. S16(b) and (d), the effect is largest in the regions where the derivative of the Köhler curve is smallest, mostly affecting the two maxima of the curve and therefore also shifting the critical point, and the droplet size where the organic film breaks. For the surface tension predictions in Fig. S16(d), the rising part of the curve is shifted with the differences decreasing with increasing droplet size. The density of the solid phase organic is the only one out of the tested parameters where the variations significantly affects the Köhler curve predictions of the simple model as shown in Fig. S16(a). The Köhler curve and the critical point is shifted, and the effect is stronger at small droplet sizes but disappears as the droplet size increases. The surface tension used in the simple model calculations (Fig. S16(c)) remains constant.

The solid phase density of the salt (ammonium sulfate) only has a very small effect on the predicted Köhler curves or surface tensions in any of the cases due to the large organic mass fraction used in these simulations. The effect would be greater if the

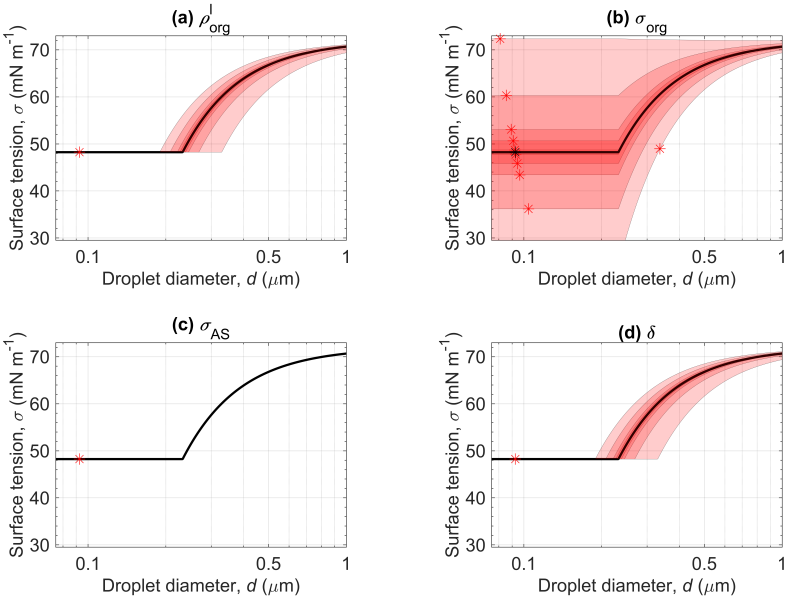

Figure S12. The sensitivity of the surface tension along the Köhler curve predicted with the partial organic film model with variations in the liquid density of the organic (a), the surface tension of pure organic compound (b), the surface tension of pure salt (c) and the thickness of the surface film (d) for particles containing malonic acid at $D_{\mathrm{p}} = 50$ nm and $w_{\mathrm{p,org}} = 0.95$. The red areas match $\pm$ 1 %, 5 %, 10 %, 25 % and 50 % variations in the parameters.

fractions of the salt in the particles were larger. In addition, variations in the liquid phase density of ammonium sulfate ($\rho^{\mathrm{l}}_{\mathrm{salt}}$) was shown not to significantly affect any of the models under these conditions.

The liquid phase density of malonic acid ($\rho^{\mathrm{l}}_{\mathrm{org}}$) was shown to only significantly affect the partial film model by modifying the point where the surface film breaks, and shifting the Köhler curve and corresponding surface tension curve afterwards (Figs. S11(a) and S12(a)). The variations of this parameter have however not affected the critical point. The monolayer model also shows very minor effects from varying the liquid phase density of the organic, as a tiny shift in the predicted Köhler curve at small droplet sizes.

S4 Thermodynamical data

S4.1 Surface tension

The surface tension on the ternary system of water, organic and ammonium sulfate used with the monolayer (Malila and Prisle, 2018), Gibbs (Prisle et al., 2010) and bulk solution models is calculated with a parameterization into ternary system data by Booth et al. (2009). The data itself was measured at at 294.15 K. The equation used for the parameterization is an extension of the Szyszkowski-Langmuir equation (Szyszkowski, 1908; Meissner and Michaels, 1949; Tuckermann, 2007)

$$\sigma = \sigma_{\mathrm{w}} - ART \ln\left(1 + \frac{x_{\mathrm{org}}}{B}\right) + Cx_{\mathrm{salt}} + Dx_{\mathrm{salt}} \ln\left(1 + \frac{x_{\mathrm{org}}}{B}\right), \tag{S9}$$

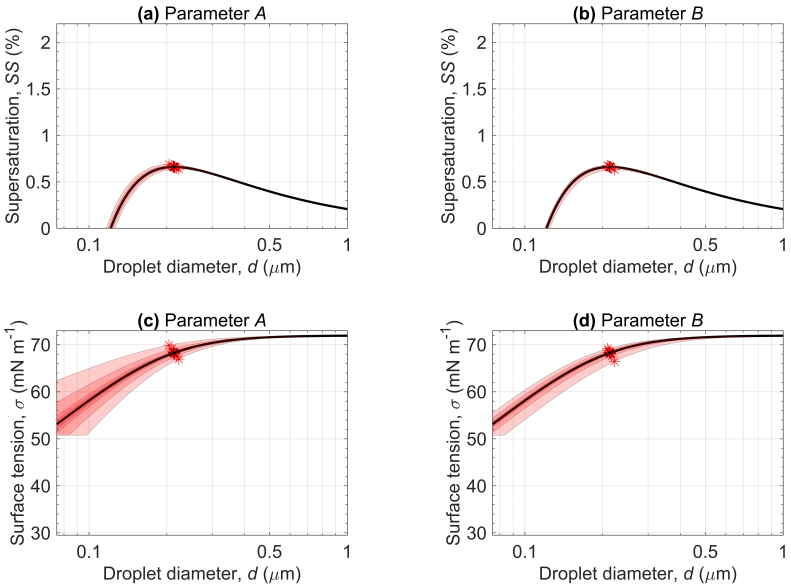

Figure S13. The sensitivity of the Köhler curve (a and b) and the surface tension along it (c and d) predicted with the bulk solution model with variations in the fitting parameters A and B in the surface tension parametrization presented in Eq. S9 and Table S6 for particles containing glutaric acid at $D_{\mathrm{p}} = 50$ nm and $w_{\mathrm{p,org}} = 0.95$. The red areas match $\pm$ 1 %, 5 %, 10 %, 25 % and 50 % changes in the parameters.

where the fitted parameters are A, B, C and D. The fit parameters for the three acids are listed in table S6 and during the simulations, the surface tension calculated by Eq.(S9) is used at 298.15 K and constrained by the pure compound as well as the binary surface tensions of water–salt and water–organic mixtures at the corresponding compositions.

The succinic and malonic acid binary fits are from Hyvärinen et al. (2006). For glutaric acid the equation is based on the measurements of Bzdek et al. (2016):

$$\sigma = \sigma_{\mathrm{w}} - 4.6485 \cdot 10^{-3} \ln(1 + 9.8319 \cdot c(x,T)), \tag{S10}$$

where the function c converts glutaric mole fraction into molarity as

$$c = \frac{x\rho(x,T)}{(xM_{\mathrm{org}} + (1-x)M_{\mathrm{w}})}, \tag{S11}$$

where ρ is the density fit for binary mixture of water and glutaric acid (Cai et al., 2015).

The surface tension of the binary mixture of water and ammonium sulfate is calculated as

$$\sigma(c,T) = \sigma_{\mathrm{w}}(T) + \frac{d\sigma}{dc}C, \tag{S12}$$

where C is the salt mass concentration and

$$\frac{d\sigma}{dc} = 0.0179 \text{ mN/m L/g} = 2.3621 \text{ mN/m L/mol}. \tag{S13}$$

The gradient was determined by combining data from Hyvärinen et al. (2005) and Aumann et al. (2010). The first point of Aumann et al. (2010) and the last two points of Hyvärinen et al. (2005) were ignored, and a least-squares fit was made into

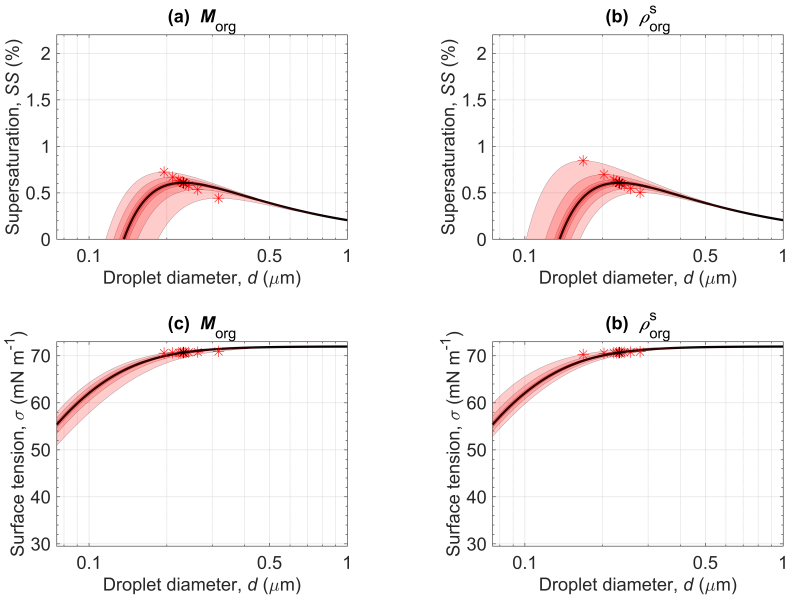

Figure S14. The sensitivity of the Köhler curve and the surface tension along it predicted with the Gibbs model with variations in the molar mass of the organic (a and c) and solid phase density of the organic (b and d) for particles containing malonic acid at $D_\mathrm{p} = 50$ nm and $w_\mathrm{p,org} = 0.95$. The red areas match $\pm$ 1 %, 5 %, 10 %, 25 % and 50 % variations in the parameters.

Eq. (S12) with the MATLAB (2019, 2020) function *fminsearch* at 298.15 K. The pure ammonium sulfate surface tension is estimated with Eq. (S12) with the mole fraction of ammonium sulfate set equal to unity. The conversion between mole fraction and mass concentration is calculated as

$$C = \frac{\rho x_\mathrm{salt}}{M_\mathrm{w}(\frac{x_\mathrm{salt}}{M_\mathrm{w}} + \frac{1-x_\mathrm{salt}}{M_\mathrm{salt}})}, \tag{S14}$$

where the aqueous ammonium sulfate density (ρ) is calculated with the equation given by Tang and Munkelwitz (1994).

The pure compound values and references are indicated in table S1 and the main article.

S4.2 Density

The density of the ternary mixture is treated as a pseudo–binary ideal mixture of water-salt and organic:

$$x_\mathrm{salt} = \frac{x_\mathrm{salt}}{x_\mathrm{w} + x_\mathrm{salt}}, \tag{S15}$$

$$M = x_\mathrm{w} M_\mathrm{w} + x_\mathrm{salt} M_\mathrm{salt}, \tag{S16}$$

$$x = x_\mathrm{w} + x_\mathrm{salt}, \tag{S17}$$

and

$$\rho = \left(\frac{Mx}{\rho_\mathrm{salt,w} \sum_j (x_j M_j)} + \frac{M_\mathrm{org} x_\mathrm{org}}{\rho_\mathrm{org} \sum_j (x_j M_j)} \right)^{-1}. \tag{S18}$$

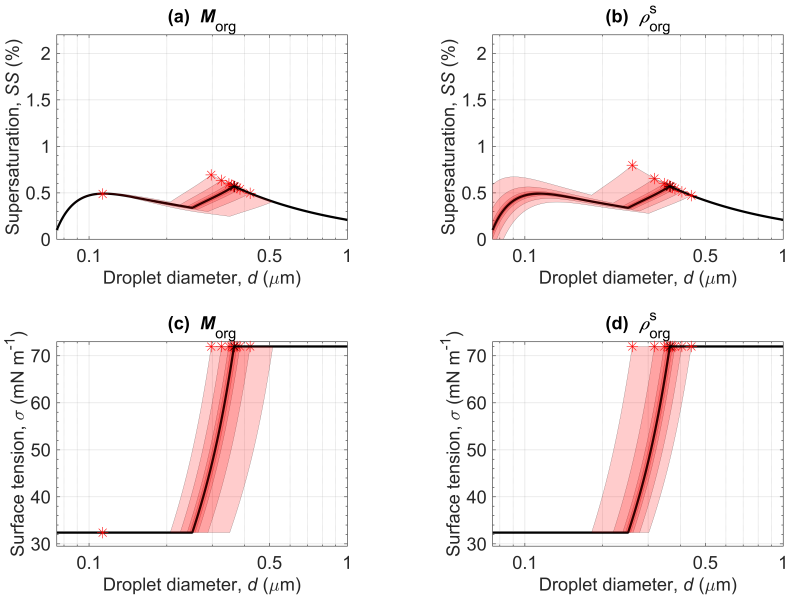

Figure S15. The sensitivity of the Köhler curve and the surface tension along it predicted with the compressed film model with variations in the molar mass of the organic (a and c) and solid phase density of the organic (b and d) for particles containing malonic acid at $D_{\mathrm{p}} = 50$ nm and $w_{\mathrm{p,org}} = 0.95$. The red areas match$\pm$ 1 %, 5 %, 10 %, 25 % and 50 % variations in the parameters.

Table S6. The ternary surface tension parameters for water, ammonium sulfate and organic needed for Eq. (S9). The fits were done into ternary system data from Booth et al. (2009) at 294.15 K and the parameters have been rounded to four decimals.

Compound	A (mol m^{-2})	B	C (Jm^{-2})	D (Jm^{-2})
Malonic	$3.2487{\cdot}10^{-6}$	0.0144	-0.0994	0.0242
Succinic	$6.5478\cdot10^{-7}$	$4.9852{\cdot}10^{-4}$	-0.3027	0.0285
Glutaric	$2.6222\cdot10^{-6}$	0.0032	-0.2271	0.0492

The binary ammonium sulfate–water mixture density ($\rho_{\mathrm{salt,w}}$) is estimated from the binary fit Tang and Munkelwitz (1994). The pure compound values and references are indicated in table S1 and the main article. The binary densities of malonic acid and succinic acid are estimated according to Hyvärinen et al. (2006) while glutaric acid follows the fit recommended by Cai et al. (2015). These are used in case there is no salt present.

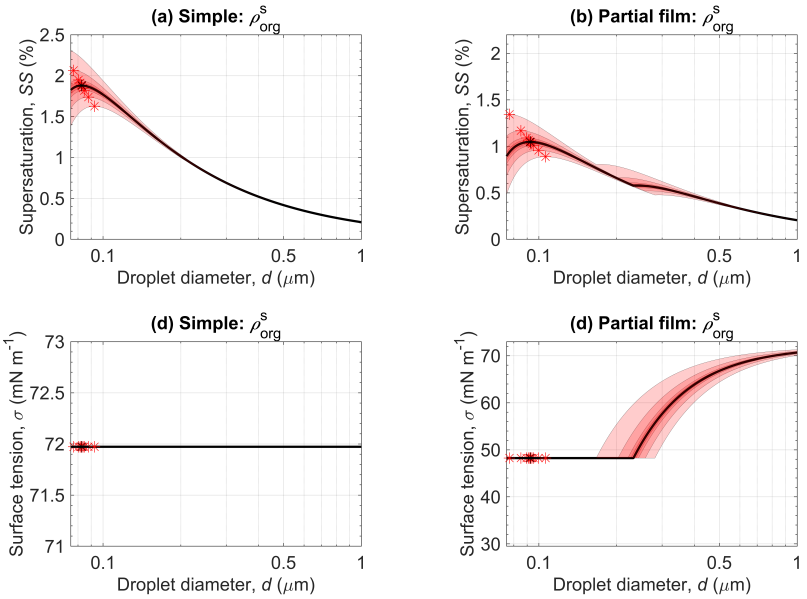

Figure S16. The sensitivity of the Köhler curve and the surface tension along it predicted with the simple and partial organic film models with variations in solid phase density of the organic (b and d) for particles containing malonic acid at $D_\mathrm{p} = 50$ nm and $w_{\mathrm{p,org}} = 0.95$. The red areas match $\pm$ 1 %, 5 %, 10 %, 25 % and 50 % variations in the parameters.

References

AIOMFAC-web: version 2.32, https://aiomfac.lab.mcgill.ca, accessed: 2020-08-19, 2020.

Aumann, E., Hildemann, L. M., and Tabazadeh, A.: Measuring and modeling the composition and temperature-dependence of surface tension for organic solutions, Atmos. Environ., 44, 329–337, https://doi.org/10.1016/j.atmosenv.2009.10.033, 2010.

Booth, A. M., Topping, D. O., McFiggans, G., and Percival, C. J.: Surface tension of mixed inorganic and dicarboxylic acid aqueous solutions at 298.15 K and their importance for cloud activation predictions, Phys. Chem. Chem. Phys., 11, 8021–8028, https://doi.org/10.1039/B906849J, 2009.

Bzdek, B. R., Power, R. M., Simpson, S. H., Reid, J. P., and Royall, C. P.: Precise, contactless measurements of the surface tension of picolitre aerosol droplets, Chem. Sci., 7, 274–285, https://doi.org/10.1039/C5SC03184B, 2016.

Cai, C., Stewart, D. J., Reid, J. P., Zhang, Y.-h., Ohm, P., Dutcher, C. S., and Clegg, S. L.: Organic Component Vapor Pressures and Hygroscopicities of Aqueous Aerosol Measured by Optical Tweezers, J. Phys. Chem. A, 119, 704–718, https://doi.org/10.1021/jp510525r, 2015.

CRC Handbook: CRC Handbook of Chemistry and Physics, 1st Student Edition, edited by Weast, R. C. , CRC Press, Boca Raton, FL., 1988.

Forestieri, S. D., Staudt, S. M., Kuborn, T. M., Faber, K., Ruehl, C. R., Bertram, T. H., and Cappa, C. D.: Establishing the impact of model surfactants on cloud condensation nuclei activity of sea spray aerosol mimics, Atmos. Chem. Phys., 18, 10 985–11 005, https://doi.org/10.5194/acp-18-10985-2018, 2018.

Frosch, M., Prisle, N. L., Bilde, M., Varga, Z., and Kiss, G.: Joint effect of organic acids and inorganic salts on cloud droplet activation, Atmos. Chem. Phys., 11, 3895–3911, https://doi.org/10.5194/acp-11-3895-2011, 2011.

Hyvärinen, A.-P., Raatikainen, T., Laaksonen, A., Viisanen, Y., and Lihavainen, H.: Surface tensions and densities of H_2SO_4 + NH_3 + water solutions, Geophys. Res. Lett., 32, L16 806, https://doi.org/10.1029/2005GL023268, 2005.

Hyvärinen, A.-P., Lihavainen, H., Gaman, A., Vairila, L., Ojala, H., Kulmala, M., and Viisanen, Y.: Surface Tensions and Densities of Oxalic, Malonic, Succinic, Maleic, Malic, and cis-Pinonic Acids, J. Chem. Eng. Data, 51, 255–260, https://doi.org/10.1021/je050366x, 2006.

Malila, J. and Prisle, N. L.: A Monolayer Partitioning Scheme for Droplets of Surfactant Solutions, J. Adv. Model. Earth Syst., 10, 3233–3251, https://doi.org/10.1029/2018MS001456, 2018.

MATLAB: version 9.6.0.1072779 (R2019a), The MathWorks Inc. [software], Natick, Massachusetts, 2019.

MATLAB: version 9.8.0.1323502 (R2020a), The MathWorks Inc. [software], Natick, Massachusetts, 2020.

Meissner, H. P. and Michaels, A. S.: Surface Tensions of Pure Liquids and Liquid Mixtures, Ind. Eng. Chem., 41, 2782–2787, https://doi.org/10.1021/ie50480a028, 1949.

Ovadnevaite, J., Zuend, A., Laaksonen, A., Sanchez, K. J., Roberts, G., Ceburnis, D., Decesari, S., Rinaldi, M., Hodas, N., Facchini, M. C., Seinfeld, J. H., and O'Dowd, C.: Surface tension prevails over solute effect in organic-influenced cloud droplet activation, Nature, 546, 637–641, https://doi.org/10.1038/nature22806, 2017.

Prisle, N. L.: Cloud Condensation Nuclei Properties of Organic Aerosol Particles: Effects of Acid Dissociation and Surfactant Partitioning, Master's thesis, University of Copenhagen, Copenhagen, https://doi.org/10.5281/zenodo.4650303, 2006.

Prisle, N. L., Raatikainen, T., Laaksonen, A., and Bilde, M.: Surfactants in cloud droplet activation: mixed organic-inorganic particles, Atmos. Chem. Phys., 10, 5663–5683, https://doi.org/10.5194/acp-10-5663-2010, 2010.

Ruehl, C. R., Davies, J. F., and Wilson, K. R.: An interfacial mechanism for cloud droplet formation on organic aerosols, Science, 351, 1447–1450, https://doi.org/10.1126/science.aad4889, 2016.

Szyszkowski, B.: Experimentelle Studien über kapillare Eigenschaften der wässerigen Lösungen von Fettsäuren., Zeitschrift für Physikalische Chemie, 64U, 385–414, https://doi.org/doi:10.1515/zpch-1908-6425, 1908.

Tang, I. N. and Munkelwitz, H. R.: Water activities, densities, and refractive indices of aqueous sulfates and sodium nitrate droplets of atmospheric importance, J. Geophys. Res. D: Atmos., 99, 18 801–18 808, https://doi.org/10.1029/94JD01345, 1994.

Tuckermann, R.: Surface tension of aqueous solutions of water-soluble organic and inorganic compounds, Atmos. Environ., 41, 6265 – 6275, https://doi.org/https://doi.org/10.1016/j.atmosenv.2007.03.051, 2007.

Vanhanen, J., Hyvärinen, A.-P., Anttila, T., Raatikainen, T., Viisanen, Y., and Lihavainen, H.: Ternary solution of sodium chloride, succinic acid and water; surface tension and its influence on cloud droplet activation, Atmos. Chem. Phys., 8, 4595–4604, https://doi.org/10.5194/acp-8-4595-2008, 2008.

Young, K. C. and Warren, A. J.: A Reexamination of the Derivation of the Equilibrium Supersaturation Curve for Soluble Particles, J. Atmos. Sci., 49, 1138–1143, https://doi.org/10.1175/1520-0469(1992)049<1138:AROTDO>2.0.CO;2, 1992.